

# Yields of AGB and SAGB models with chemistry of low– and high–metallicity Globular Clusters

P. Ventura<sup>1\*</sup>, M.Di Criscienzo<sup>3</sup>, R.Carini<sup>1,2</sup> and F. D’Antona<sup>1</sup>

<sup>1</sup>*INAF-Osservatorio Astronomico di Roma, Via Frascati 33, Monte Porzio Catone 00040, Italy*

<sup>2</sup>*Dipartimento di Fisica, Università di Roma “La Sapienza”, Italy*

<sup>3</sup>*INAF-Osservatorio Astronomico di Capodimonte, Salita Moiariello 16, Napoli 80131, Italy*

Accepted, Received; in original form

## ABSTRACT

We present yields from stars of mass in the range  $M_{\odot} \leq M \leq 8M_{\odot}$  of metallicities  $Z = 3 \times 10^{-4}$  and  $Z = 8 \times 10^{-3}$ , thus encompassing the chemistry of low– and high– $Z$  Globular Clusters. The yields are based on full evolutionary computations, following the evolution of the stars from the pre–Main Sequence through the Asymptotic Giant Branch phase, until the external envelope is lost.

Independently of metallicity, stars with  $M < 3M_{\odot}$  are dominated by Third Dredge–Up, thus ejecting into their surroundings gas enriched in carbon and nitrogen. Conversely, Hot Bottom Burning is the main responsible for the modification of the surface chemistry of more massive stars, whose mass exceeds  $3M_{\odot}$ : their gas shows traces of proton–capture nucleosynthesis.

The extent of Hot Bottom Burning turns out to be strongly dependent on metallicity. Models with  $Z = 8 \times 10^{-3}$  achieve a modest depletion of oxygen, barely reaching  $-0.3$  dex, and do not activate the Mg–Al chain. Low– $Z$  models with  $Z = 3 \times 10^{-4}$  achieve a strong nucleosynthesis at the bottom of the envelope, with a strong destruction of the surface oxygen and magnesium; the most extreme chemistry is reached for models of mass  $\sim 6M_{\odot}$ , where  $\delta[\text{O}/\text{Fe}] \sim -1.2$  and  $\delta[\text{Mg}/\text{Fe}] \sim -0.6$ . Sodium is found to be produced in modest quantities at these low  $Z$ ’s, because the initial increase due to the combined effect of the second dredge–up and of  $^{22}\text{Ne}$  burning is compensated by the later destruction via proton capture. A great increase by a factor  $\sim 10$  in the aluminium content of the envelope is also expected. These results can be used to understand the role played by intermediate mass stars in the self–enrichment scenario of globular clusters: the results from spectroscopic investigations of stars belonging to the second generation of clusters with different metallicity will be used as an indirect test of the reliability of the present yields.

The treatment of mass loss and convection are confirmed as the main uncertainties affecting the results obtained in the context of the modeling of the thermal pulses phase. An indirect proof of this comes from the comparison with other investigations in the literature, based on a different prescription for the efficiency of convection in transporting energy and using a different recipe to determine the mass loss rate.

**Key words:** Stars: abundances – Stars: AGB and post-AGB

## 1 INTRODUCTION

Stars with mass below  $6M_{\odot}$ , shortly after the end of core helium burning, develop a degenerate core of Carbon and Oxygen, and evolve supported by two nuclear regions, where CNO and  $3\alpha$  burning occur. Due to the narrow dimensions of the He–burning layer,  $3\alpha$  burning is not thermally stable (Schwarzschild & Harm 1965, 1967), and occurs period-

ically, in violent episodes known as thermal pulses (hereinafter TP); for most of the time CNO burning is the only energy channel active in the star (Iben 1975). In the Hertzsprung–Russell diagram, the evolutionary tracks, after the excursion to the blue during the core He–burning phase, turn again to the red; this evolutionary phase is commonly known as Asymptotic Giant Branch (AGB).

More massive objects, with mass  $6M_{\odot} < M < 8M_{\odot}$ ,

\* E-mail: paolo.ventura@oa-roma.inaf.it (AVR)

<sup>1</sup> These limits in mass partly depend on the assumption concern-

undergo a similar evolution, with the difference that their internal temperatures are sufficiently high to trigger carbon ignition in a partially degenerate region, near the stellar center (Ritossa et al. 1996, 1999). In these stars the inwards propagation of a convective flame favors the formation of a core made up of oxygen and neon. Like their lower mass counterparts, they also undergo a series of thermal pulses, and evolve in the Super Asymptotic Giant Branch (SAGB) phase (Siess 2006, 2007, 2010).

The fate of AGB stars is to eventually lose their envelope, and evolve to the White Dwarf stage. The final stages of the evolutionary history of SAGBs is more uncertain. If the mass loss rate is low, their core grows in mass until exceeding the Chandrasekhar limit, thus favoring the conditions for core-collapse supernova, via electron capture. Alternatively, they evolve as ONe white dwarfs (Poelarends et al. 2008).

The AGB evolution is rather short compared to the previous phases of core burning, but it proves extremely important because it is during this phase that most of the mass is lost from the star. Understanding the evolution of the surface chemistry of these stars is crucial for a number of topics, such as the role played by AGBs and SAGBs as dust producers (Gail & Sedlmayr 1999; Ferrarotti & Gail 2006), that was shown to depend critically on the abundances of the various chemical species in the surface layers of the star (Ventura et al. 2012a,b).

AGB and the SAGB stars have been invoked to explain the observations of stars in Globular Clusters (GC) (Ventura et al. 2001). The spectroscopic and photometric results gathered in the last decades indicate the presence of multiple populations (Carretta et al. 2009; Gratton et al. 2001; D'Antona et al. 2005; Piotto et al. 2007), and that (at least) a new generation of stars formed from the ashes of rapidly evolving stars belonging to the original population of the cluster. Massive AGBs and SAGBs appear to be the most appealing candidates, in spite of an ongoing debate, due to the various uncertainties affecting the robustness of the results of AGB modeling. This is the reason why some research groups argued against the possibility that AGB winds could ever reproduce the chemical patterns observed (Fenner et al. 2004), whereas other investigations showed that on the qualitative side the most massive AGBs produce ejecta whose chemistry is in agreement with the anticorrelations observed (Ventura & D'Antona 2009).

The investigations by D'Ercole et al. (2008, 2010, 2011, 2012) set the theoretical framework to describe the formation of a second generation of stars in GCs, by gas ejected by AGB and SAGB stars, diluted with pristine gas having the original chemistry. These studies outlined the importance of the role played by SAGBs: these stars evolve rapidly, and their winds could give origin to the formation of a He-rich stellar component, whose presence is suggested by photometric investigations of some GCs.

The yields from SAGBs are therefore crucial for this study. The spectroscopic analysis of stars belonging to the

ing the extent of the extra-mixing region from the external border of the convective core during the hydrogen burning phase. In the present investigation we consider a modest overshoot; if this was neglected, the range of masses involved in the SAGB evolution would be  $8M_{\odot} < M < 10M_{\odot}$

blue MS of GCs constitute a valuable test of the self-enrichment by AGBs mechanism, because their surface chemistry should reflect the composition of the yields of SAGBs.

Our previous investigations on this topic were based on a single metallicity,  $Z=0.001$ , corresponding to the chemistry of GCs with intermediate metallicity (Ventura & D'Antona 2009, 2011). This limitation was caused by lack of SAGB models of different metallicity, with the exception of the compilation by Siess (2010). To allow a more complete analysis we present here AGB and SAGB models spanning the range of metallicities of GCs, ranging from the chemistry typical of low-metallicity GCs,  $Z = 3 \times 10^{-4}$ , to the more metallic clusters, i.e.  $Z = 8 \times 10^{-3}$ .

Although we discuss the implications for the self-enrichment by AGB & SAGB stars, this investigation is focused on the properties of the models, while the analysis of how these new yields compare with the observations of the GCs of the same metallicity is postponed to future investigations.

## 2 THE MODELS

The models presented and discussed in this paper were calculated by means of the ATON code for stellar evolution. A detailed description of the numerical structure of the code can be found in Ventura et al. (1998).

The metallicities investigated are  $Z = 8 \times 10^{-3}$  and  $Z = 3 \times 10^{-4}$ . The mixtures follow the relative abundances of the elements according to Grevesse & Sauval (1998), with  $\alpha$ -enhancement  $[\alpha/\text{Fe}] = +0.2$  (for  $Z = 8 \times 10^{-3}$ ) and  $[\alpha/\text{Fe}] = +0.4$  (for  $Z = 3 \times 10^{-4}$ ). These choices correspond to  $[\text{Fe}/\text{H}] = -0.5$  and  $[\text{Fe}/\text{H}] = -2$ , typical of high metallicity GCs, such as NGC 6388, and low-metallicity structures, such as NGC 2419.

Convection was modelled in all cases by means of the Full Spectrum of Turbulence (FST) model, presented by Canuto & Mazzitelli (1991). The impact of this choice has been discussed extensively in the literature (e.g. Ventura & D'Antona 2005), and will not be repeated here.

In convectively unstable regions nuclear burning and mixing of chemicals were coupled by means of a diffusive approach, using the scheme by Cloutmann & Eoll (1976). Overshoot of convective eddies into radiatively stable regions is modelled by assuming an exponential decay of convective velocities starting from the convective borders; the e-folding distance of this behavior is given by  $\sim \zeta H_P$ , where  $\zeta$  is the free parameter measuring the extent of the extra-mixing. During the two main phases of core burning we assumed  $\zeta = 0.02$ , in agreement with Ventura et al. (1998). We further explore the effects of a tiny extra-mixing from the convective shell that forms during the ignition of each thermal pulse (Pulse Driven Convective Shell, hereinafter PDCS) by comparing the results obtained by neglecting any extra-mixing during the AGB evolution, with those found by assuming  $\zeta = 0.001$ : this assumption was found to enhance the strength of thermal pulses, and to an increase in the inwards penetration of the external mantle during the post-pulse phases (Herwig 2000). No overshoot was assumed from the bottom of the convective envelope during the AGB phase. These choices, far from being a true cali-

bration of a still largely unknown physical phenomenon, are intended to have a rough estimate on how the extent of the third dredge-up, and consequently the yields of the elements discussed in this investigation, depend on the various factors that favor an enhancement of the inwards penetration of the convective envelope in the phases following the thermal pulse. A much more detailed treatment would be required for those phenomena strongly dependent on the details of such a penetration, such as the s-process enrichment.

Mass loss was modelled according to Blöcker (1995). The free parameter entering this recipe was set to  $\eta_R = 0.02$ , in agreement with the calibration based on the luminosity function of lithium-rich stars in the Magellanic Clouds given by Ventura et al. (2000). The Blöcker description is based on a steep dependence of  $\dot{M}$  on luminosity,  $\dot{M} \sim L^{4.7}$ , in agreement with dynamical models of AGB envelopes by Bowen (1988). For M stars, with masses  $M > 4M_\odot$ , evolving at large luminosities, the mass loss rates used here are substantially larger than other treatments in the literature, such as the classic recipe by Vassiliadis & Wood (1993), or the empirical relation by Van Loon et al. (2005); this difference will result in a smaller number of thermal pulses. For models of smaller mass, the comparison between the Blöcker formula and the treatment for C-star winds by Wachter et al. (2002) is mainly determined by the strong sensitivity to the effective temperature ( $\sim T_{eff}^{6.81}$ ) of this latter. In this mass interval the mass loss rates used here are smaller, although a comparison with other investigations in the literature is not trivial, because the effects of the mass loss treatment are strongly related to the way convection is modelled, which is relevant for the effective temperature of the models.

Radiative opacities for temperatures above 10000K were computed by the OPAL release, in the version documented by Iglesias & Rogers (2006). In the low temperature regime we use the AESOPUS tool by Marigo & Aringer (2009), that allows to account for changes in the surface chemistry determined by TDU and HBB. Though more time consuming, this choice is mandatory for a reliable description of the evolutionary phases during the AGB evolution that follow the carbon enrichment of the external layers, as discussed in details in Ventura & Marigo (2009, 2010). The conductive opacities were taken from Potekhin (2006)<sup>2</sup>, and are added harmonically to the radiative opacities.

Tables of the equation of state are generated in the (gas) pressure-temperature plane, according to the latest release of the OPAL EOS (2005), overwritten in the pressure ionization regime by the EOS by Saumon et al. (1995), and extended to the high-density, high-temperature domain according to the treatment by Stolzmann & Blöcker (2000).

The relevant cross-sections are taken from the recommended values in the NACRE compilation (Angulo et al. 1999), with only the following exceptions:  $3\alpha$  (Fynbo et al. 2005);  $^{12}\text{C}(\alpha,\gamma)^{16}\text{O}$  (Kunz et al. 2002);  $^{14}\text{N}(\text{p},\gamma)^{15}\text{O}$  (Formicola et al. 2004);  $^{22}\text{Ne}(\text{p},\gamma)^{23}\text{Na}$  (Hale et al. 2002);  $^{23}\text{Na}(\text{p},\gamma)^{24}\text{Mg}$  (Hale et al. 2004);  $^{23}\text{Na}(\text{p},\alpha)^{20}\text{Ne}$  (Hale et al. 2004);  $^{25}\text{Mg}(\text{p},\gamma)^{26}\text{Al}$  (NACRE, upper limits);  $^{26}\text{Mg}(\text{p},\gamma)^{27}\text{Al}$  (NACRE, upper limits).

### 3 AGB AND SAGB EVOLUTION: PHYSICAL ASPECTS

The evolutions presented in this work have been followed from the pre-main sequence throughout the AGB phase, until the almost complete ejection of the external envelope. The evolution of models developing a degenerate core, and experiencing the helium flash, were stopped at the tip of RGB, and resumed with an artificial HB model, having the same core mass as the model at the RGB tip. For  $Z = 3 \times 10^{-4}$  the helium flash was experienced by models with mass below  $2M_\odot$ , whereas for  $Z = 8 \times 10^{-3}$  the threshold mass is  $M < 2.5M_\odot$ .

Table 1 summarizes the main physical quantities of the models discussed here, and the average chemistry of their ejecta. We also report the results for  $Z = 10^{-3}$  by Ventura & D’Antona (2009, 2011), and Ventura & Marigo (2010). The first seven columns contain information regarding the physical evolution of the models: initial mass (solar units), time after which the AGB phase begins (yr), number of thermal pulses experienced, inter-pulse period (yr), core masses at the first TP and at the maximum in luminosity (solar units), and maximum temperature reached by the bottom of the convective envelope. Cols. 8–16 give information on the average composition of the ejecta, that is the helium mass fraction, the lithium content (expressed in the standard notation for lithium, i.e.  $\log \epsilon(\text{Li}) = \log(n(\text{Li})/n(\text{H})) + 12$ ), and the abundances of the elements mostly investigated in the spectroscopic surveys of GC stars, i.e. the CNO elements, sodium, magnesium (where we intend the sum of the three isotopes), aluminium and silicon. The abundances from carbon to silicon are given as  $[i/\text{Fe}] = \log(X_i/X_{\text{Fe}}) - \log(X_i/X_{\text{Fe}})_\odot$ , to allow a more straight comparison with the observations.

The two panels of Fig. 1 show the main physical properties of the AGB evolution of the models computed: in the left panel we show the highest luminosity reached during the AGB phase as a function of the corresponding core mass, whereas in the right panel we report the highest temperature reached at the bottom of the convective mantle.

The trend of luminosity with core mass is rather similar for the two metallicities, with the exception of the models within the SAGB regime: the lower metallicity models reach larger luminosities.

In the right panel of Fig. 1 we see a clear gap in temperature separating low-mass models, with core masses below  $0.8M_\odot$ , from their higher mass counterparts. These latter experience Hot Bottom Burning (hereinafter HBB), consisting in the nuclear activity at the bottom of the convective envelope when the temperature exceeds 30 – 40MK. HBB favours a rapid increase in the luminosity of the star (Blöcker & Schönberner 1991), and its description depends on the details of convection modelling (Renzini & Voli 1981; Boothroyd & Sackmann 1988). The threshold mass to achieve HBB is  $3M_\odot$  and  $3.5M_\odot$ , respectively, for the  $Z = 3 \times 10^{-4}$  and  $Z = 8 \times 10^{-3}$  cases. As will be discussed in more details in the following sections, HBB ignition has a strong influence on the chemical patterns. Models experiencing HBB evolve at large luminosities, and loose their envelope much faster; compared to the lower masses, they undergo a limited number of thermal pulses, so that the ef-

<sup>2</sup> See the web page [www.ioffe.rssi.ru/astro/conduct/](http://www.ioffe.rssi.ru/astro/conduct/)

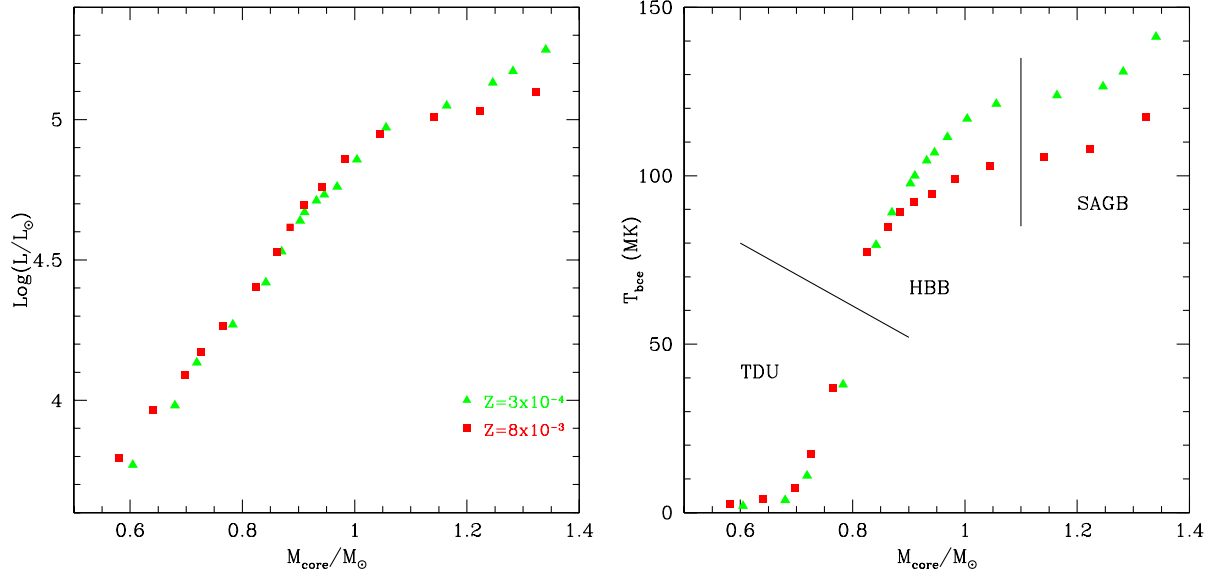


**Figure 1.** The maximum luminosity achieved during the AGB evolution (left), and the maximum temperature reached at the bottom of the surface convective zone (right) as a function of the core mass, for models with metallicity  $Z = 3 \times 10^{-4}$  (blue triangles) and  $Z = 8 \times 10^{-3}$  (red squares).

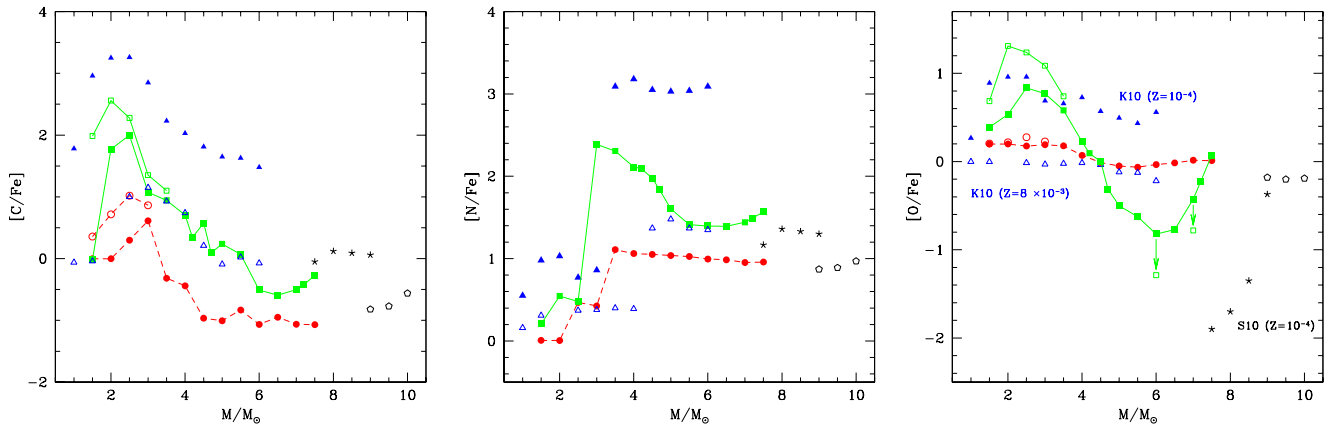


**Figure 2.** Average content of carbon (left panel), nitrogen (middle), oxygen (right) for AGB and SAGB models of different metallicity, and with different treatment of the borders of the convective shell that forms when the thermal pulses occur. Models presented in this investigation with metallicity  $Z = 3 \times 10^{-4}$  and  $Z = 8 \times 10^{-3}$  are indicated, respectively in green (full squares) and red (full dots); the same models, where some extra-mixing was assumed from the borders of the PDCS are indicated with open squares and dots. The Blue points indicated models by Karakas (2010) of metallicity  $Z = 10^{-4}$  (full triangles) and  $Z = 8 \times 10^{-3}$  (open triangles). Black asterisks and open points indicated the results by Siess (2010) with chemistry, respectively,  $Z = 10^{-4}$  and  $Z = 8 \times 10^{-3}$ .

fects of TDU in the alteration of the surface chemistry is modest (Ventura & D'Antona 2008).

Models whose core-mass exceeds  $1.1M_{\odot}$  ignite carbon in an off-center, partially degenerate region, and evolve as SAGB stars.

The right panel of Fig. 1 confirms that the strength of HBB is extremely sensitive to metallicity. The  $T_{bce}$  vs  $M_{core}$  trend of the two sets of models discussed here differ in the HBB domain. While in the  $Z = 8 \times 10^{-3}$  models the temperature at the bottom of the external mantle hardly reaches 100MK, in all low- $Z$  models undergoing HBB we find  $T_{bce} > 100MK$ , with a maximum temperature, approaching 150MK, reached inside the  $7.5M_{\odot}$  model. This is going to

have a great impact on the extent of the nucleosynthesis experienced, given the extreme sensitivity to T of the cross-section of the various proton capture channels around  $\sim 100MK$ .

As discussed in section 2, the results obtained depend on the choices made to model convection and mass loss. The treatment of convection is essential in determining the strength of HBB: the range of masses experiencing HBB would be narrower if a lower-efficiency convection model, such as the Mixing Length Theory, would be used. Mass loss has no influence in determining whether HBB occurs for a given mass or not. However, changing the mass loss rate alters the rapidity with which mass loss occurs, hence

**Table 1.** Relevant properties of AGB models

M	$\tau_{\text{evol}}$	$N_p$	$\tau_i$	$M_c^{1TP}$	$M_c$	$T_{\text{bce}}^{\text{max}}$	Y	Li	C	N	O	Na	Mg	Al	Si
$Z = 3 \times 10^{-4}$															
1.5	1.06e9	13	1.5e5	0.58	0.68	4e6	0.27	-1.03	1.99	0.27	0.69	0.19	0.42	0.12	0.40
2.0	8.05e8	21	1.0e5	0.59	0.72	1.1e7	0.28	1.06	2.56	0.59	1.31	0.86	0.78	1.00	0.40
2.5	4.55e8	22	3.0e4	0.72	0.78	3.8e7	0.26	1.17	2.28	0.52	1.24	0.66	0.73	1.09	0.41
3.0	2.94e8	27	1.3e4	0.80	0.84	7.9e7	0.27	2.82	1.35	2.59	1.09	1.62	0.61	0.93	0.41
3.5	2.07e8	34	8.5e3	0.83	0.87	8.9e7	0.27	2.33	0.36	1.87	0.49	1.10	0.42	0.40	0.41
4.0	1.55e8	41	5.5e3	0.86	0.90	9.8e7	0.29	2.06	0.12	1.76	0.19	0.91	0.37	0.76	0.41
4.2	1.38e8	42	5.1e3	0.88	0.91	1.e8	0.33	2.27	0.35	2.10	0.09	0.83	0.25	1.12	0.42
4.5	1.20e8	47	3.6e3	0.90	0.93	1.02e8	0.33	2.14	0.23	1.94	-0.13	0.61	0.07	1.16	0.46
4.7	1.09e8	49	2.8e3	0.91	0.95	1.07e8	0.34	2.02	0.10	1.83	-0.31	0.41	-0.05	1.21	0.53
5.0	9.60e7	53	2.1e3	0.94	0.97	1.11e8	0.35	2.05	0.24	1.60	-0.50	0.19	-0.18	1.04	0.61
5.5	7.90e7	54	1.3e3	0.98	1.00	1.17e8	0.36	1.95	0.07	1.41	-0.62	0.03	-0.13	0.89	0.63
6.0	6.70e7	41	1.0e3	1.02	1.05	1.21e8	0.36	1.90	-0.51	1.40	-0.82	0.01	0.02	0.86	0.59
6.5	5.70e7	39	4.5e2	1.14	1.16	1.24e8	0.36	1.58	-0.59	1.39	-0.77	-0.04	0.07	0.86	0.57
7.0	4.95e7	37	3.2e2	1.21	1.25	1.27e8	0.37	1.89	-0.50	1.44	-0.43	0.08	0.22	0.82	0.51
7.2	4.70e7	35	2.9e2	1.25	1.28	1.31e8	0.37	2.17	-0.43	1.49	-0.23	0.29	0.27	0.75	0.49
7.5	4.35e7	31	2.6e2	1.30	1.34	1.41e8	0.37	3.17	-0.27	1.57	0.07	0.81	0.35	0.60	0.44
$Z=10^{-3}$															
2.0	9.70e8	20	2.1e5	0.53	0.69	7e6	0.26	1.44	1.45	0.48	0.56	0.33	0.41	0.13	0.40
2.5	5.35e8	21	6.7e4	0.64	0.74	1.8e7	0.25	0.44	1.68	0.51	0.98	0.39	0.49	0.59	0.40
3.0	3.40e8	26	1.8e4	0.77	0.82	6.5e7	0.25	2.53	0.84	2.21	0.92	1.16	0.57	0.65	0.40
3.5	2.35e8	31	1.2e4	0.81	0.85	8.3e7	0.26	2.33	0.51	2.18	0.77	1.30	0.55	0.66	0.40
4.0	1.74e8	34	7.9e3	0.84	0.88	8.9e7	0.28	2.06	0.14	2.02	0.44	1.18	0.48	0.55	0.40
4.5	1.33e8	39	5.3e3	0.87	0.91	9.5e7	0.31	1.89	0.12	1.89	0.19	0.97	0.41	0.96	0.41
5.0	1.06e8	40	3.0e3	0.91	0.94	1.01e8	0.32	1.97	0.13	1.70	-0.06	0.60	0.35	1.02	0.43
5.5	8.48e7	41	2.0e3	0.96	0.98	1.06e8	0.33	1.99	-0.41	1.51	-0.35	0.37	0.28	1.10	0.44
6.0	7.11e7	34	1.2e3	1.00	1.03	1.12e8	0.34	2.18	-0.62	1.35	-0.40	0.31	0.27	1.04	0.45
6.3	6.50e7	33	7.9e2	1.03	1.06	1.14e8	0.35	2.22	-0.68	1.33	-0.37	0.30	0.30	0.99	0.44
6.5	6.07e7	32	5.0e2	1.10	1.12	1.16e8	0.35	2.36	-0.71	1.31	-0.24	0.32	0.23	0.80	0.44
7.0	5.26e7	31	4.1e2	1.18	1.20	1.2e8	0.36	2.12	-0.69	1.31	-0.15	0.39	0.25	0.74	0.44
7.5	4.62e7	29	2.9e2	1.25	1.28	1.27e8	0.36	2.75	-0.61	1.31	0.01	0.67	0.29	0.57	0.43
8.0	4.18e7	28	2.1e2	1.32	1.34	1.36e8	0.35	4.39	0.23	1.31	0.20	1.00	0.29	0.40	0.42
$Z=8 \times 10^{-3}$															
1.5	2.44e9	14	1.5e5	0.54	0.64	4e6	0.28	-2.73	0.36	0.01	0.21	0.10	0.20	0.00	0.20
2.0	1.06e9	18	1.3e5	0.55	0.70	7e6	0.28	-2.51	0.72	0.01	0.22	0.16	0.21	0.00	0.20
2.5	6.98e8	28	1.7e5	0.51	0.73	1.7e7	0.28	1.95	1.02	0.46	0.28	0.28	0.24	0.17	0.20
3.0	4.13e8	28	7.0e4	0.62	0.76	3.7e7	0.28	1.31	0.86	0.42	0.23	0.25	0.23	0.18	0.20
3.5	2.68e8	32	6.0e4	0.76	0.82	7.7e7	0.28	2.90	-0.32	1.11	0.18	0.85	0.22	0.16	0.20
4.0	1.89e8	35	9.0e3	0.82	0.86	8.5e7	0.29	2.71	-0.44	1.06	0.07	0.81	0.20	0.15	0.20
4.5	1.42e8	33	6.0e3	0.85	0.88	8.9e7	0.31	2.58	-0.97	1.05	-0.01	0.76	0.20	0.18	0.20
5.0	1.11e8	37	4.0e3	0.88	0.91	9.2e7	0.32	2.35	-1.00	1.04	-0.05	0.71	0.19	0.23	0.20
5.5	8.93e7	40	2.4e3	0.92	0.94	9.5e7	0.34	2.59	-0.83	1.03	-0.06	0.67	0.19	0.27	0.20
6.0	7.38e7	29	1.5e3	0.96	0.98	9.9e7	0.35	2.63	-1.06	1.00	-0.03	0.65	0.19	0.25	0.20
6.5	6.20e7	39	8.5e2	1.02	1.04	1.03e8	0.36	2.93	-0.95	0.99	-0.01	0.65	0.19	0.25	0.20
7.0	5.32e7	24	6.0e2	1.12	1.14	1.05e8	0.36	3.27	-1.06	0.95	0.02	0.66	0.20	0.19	0.20
7.5	4.64e7	21	4.2e2	1.20	1.22	1.08e8	0.37	2.98	-1.07	0.96	0.01	0.68	0.20	0.18	0.20
8.0	4.09e7	20	2.9e2	1.30	1.32	1.16e8	0.37	3.91	-1.08	0.93	0.04	0.74	0.19	0.18	0.20

the number of TPs experienced. For models experiencing HBB, we have seen that the Blöcker's recipe used here leads to mass loss rates in excess with other treatments in the literature: this favours a faster AGB evolution, and the contamination of the surface chemistry determined by HBB will be softer, because there is no time of achieving a very advanced nucleosynthesis. In the low-mass regime, for models reaching the C-star stage, our recipe for mass loss leads to smaller rates: this reflects in a difference in the final core

mass of the models, which is  $\sim 0.01 - 0.02M_{\odot}$  larger in the present case.

#### 4 YIELDS FROM AGBS AND SAGBS

The surface chemistry of AGBs is modified by TDU and HBB. The results obtained change dramatically according to which of these two mechanisms is dominant, given the different chemical patterns produced. TDU determines an

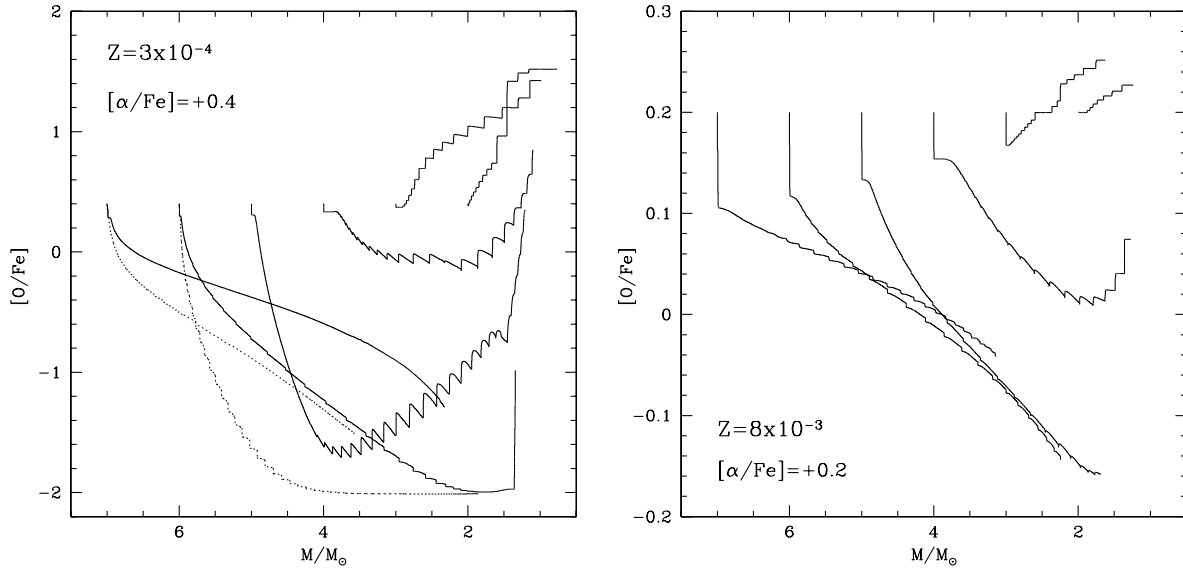


**Figure 3.** The variation of the surface oxygen during the AGB evolution of stars of different mass, and metallicity  $Z = 3 \times 10^{-4}$  (left panel) and  $Z = 8 \times 10^{-3}$  (right). The initial abundances of oxygen, in agreement with the choice for the  $\alpha$ -enhancement of the two mixtures, are  $[O/Fe]=+0.4$  ( $Z = 3 \times 10^{-4}$ ) and  $[O/Fe]=+0.2$  ( $Z = 8 \times 10^{-3}$ ). The effects of the second dredge-up can be seen in the decrease in the oxygen content of the envelope at the beginning of the AGB evolution. The two dotted lines in the left panel indicate the results concerning two low- $Z$  models with initial mass  $6M_{\odot}$  and  $7M_{\odot}$ , calculated with a smaller rate of mass loss. Use of different scales was made compulsory by the different extent of both TDU and HBB for the two metallicities.

increase in the surface carbon, possibly followed by nitrogen synthesis via proton capture during the quiescent phase of CNO burning. HBB changes the chemical composition according to the equilibrium abundances associated to p-capture nucleosynthesis; this is extremely sensitive to the temperature at which HBB occurs. A fundamental difference between the effects of these two mechanisms is that the overall C+N+O keeps constant as far as HBB dominates, whereas it increases if repeated TDU episodes occur.

#### 4.1 CNO

The surface content of carbon, nitrogen and oxygen is touched by both TDU and HBB. In the three panels of Fig. 2 we show the average content of C (left), N (middle), O (right) in the ejecta of stars with initial mass in the range  $M_{\odot} \leq M \leq 8M_{\odot}$ . To allow a more straight comparison with the spectroscopic analysis of stars in Globular Clusters, we show in the ordinate, for each element  $i$ , the quantity  $[i/Fe]$ . For a solar-scaled mixture, a positive  $[i/Fe]$  indicates a production of the  $i$ -th element, whereas a negative value means that the element was destroyed. Note that for oxygen, which is an  $\alpha$ -element, the threshold values separating the production and destruction regimes are +0.2 and +0.4, respectively, for  $Z = 8 \times 10^{-3}$  and  $Z = 3 \times 10^{-4}$ . The same holds for magnesium and silicon.

The  $Z = 8 \times 10^{-3}$  models, indicated with red circles, are connected with dashed lines; the results for  $Z = 3 \times 10^{-4}$  are indicated with squares, connected with solid lines. In the low-mass regime, full points indicate the results obtained by neglecting extra-mixing from the convective shell formed during the thermal pulses; models with some extra-mixing are indicated with open points. Because this differ-

ence mainly reflects on the efficiency of the TDU, it has no influence in the high-mass domain, where the chemistry is mostly determined by HBB.

$[C/Fe]$  increases with mass in the low-mass domain (see left panel of Fig 2); this holds independently of metallicity, and is due to the higher number of thermal pulses experienced by higher mass models, allowing a greater enrichment in the surface carbon. The yields of lower  $Z$  models are predicted to be much richer in carbon, because mixing is more efficient in low metallicity models (Boothroyd & Sackmann 1988); also, for a given penetration of the surface convection determined by TDU, the percentage increase in the abundance of a given element is larger the lower is  $Z$ .

Independently of the metallicity, assuming some extra-mixing from the borders of the PDCS, in agreement with the results by Herwig (2000), favors the inwards penetration of the base of the envelope in the post-pulse phase, thus leading to a more efficient TDU. The carbon yields are consequently enhanced by a factor  $\sim 10$ .

In models experiencing HBB carbon is destroyed during the interpulse phase, which is the reason for the negative trend with mass, shown in the left panel of Fig. 2. The  $Z = 3 \times 10^{-4}$  models, though experiencing a stronger HBB (see right panel of Fig. 1), show a higher carbon content, because of the effects of late TDU episodes, that increase the surface carbon content in the evolutionary phases preceding the White Dwarf cooling, just before the whole envelope is lost.

Nitrogen is not directly touched by TDU, which refurbishes the envelope of carbon and (in minor quantities) of oxygen. This is the reason why models with mass below 2–2.5 $M_{\odot}$  show only a modest (if any) enhancement of nitrogen (see the middle panel of Fig. 2). The average nitrogen in the

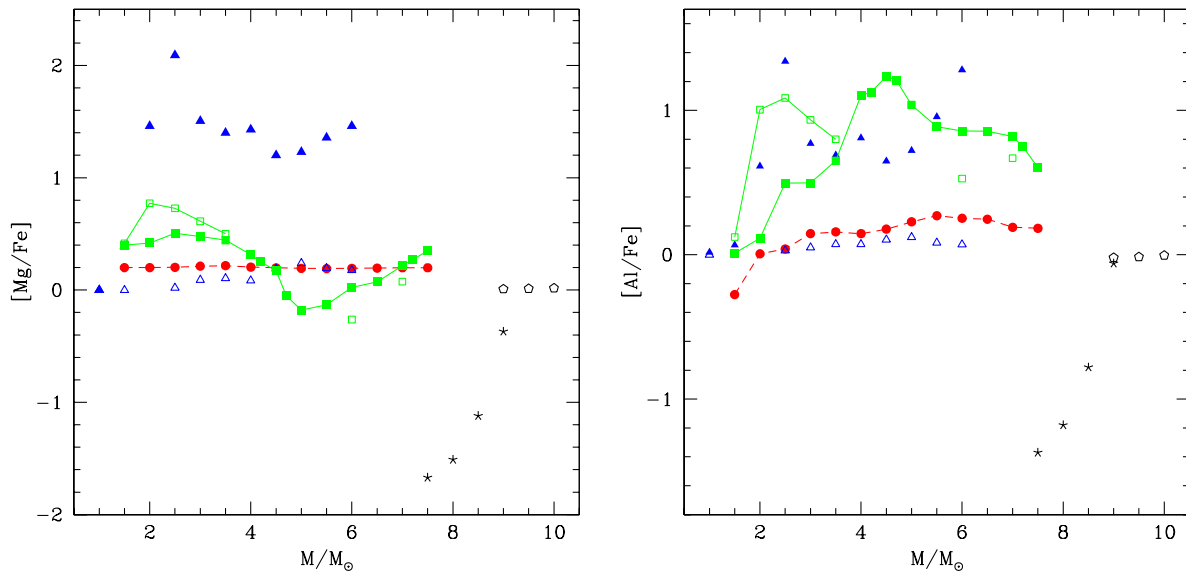


**Figure 4.** Average magnesium (left) and aluminium (right) content of the ejecta of models presented in this investigation, compared to results by Karakas (2010) and Siess (2010). The meaning of symbols is the same as in Fig. 2.

ejecta shows a sharp increase for masses around the threshold value separating the TDU from the HBB regime: in these models, the carbon carried to the surface by TDU is later converted into nitrogen during the interpulse phase.

Low  $Z$  models, experiencing a deeper TDU and a stronger HBB, are more efficient nitrogen manufacturers. N is increased by a factor  $\sim 300$  in the  $Z = 3 \times 10^{-4}$  models experiencing both TDU and HBB, and by a factor  $\sim 15$  in  $Z = 8 \times 10^{-3}$  models.

Higher mass models, experiencing only HBB, achieve a smaller production of nitrogen: in this case the increase is only due to the conversion of the carbon and oxygen originally present in the gas, with no additional contribution from TDU.

Unlike carbon, the predictions regarding the nitrogen content of the ejecta are more robust, and much less sensitive to the quantity of extra-mixing assumed from the borders of the PDCS. The influence of this latter is limited to the models achieving the maximum production of nitrogen, and is at most a factor  $\sim 2$  for masses  $M \sim 2.5 - 3M_{\odot}$ .

Oxygen is a key-element in the interpretation of the physical processes that alter the surface chemical composition of AGBs: TDU produces a positive oxygen yield, whereas HBB destroys it. The variation of the surface oxygen in some of the models discussed here is shown in Fig. 3. The choice of the mass of the star (decreasing during the evolution) as abscissa allows a better understanding of the average chemistry of the yields.

The solid and dashed lines in the right panel of Fig. 2 (indicating, respectively, the metallicities  $Z = 3 \times 10^{-4}$  and  $Z = 8 \times 10^{-3}$ ), trace similar patterns, with the difference that the lower- $Z$  line is more stretched both upwards and downwards. Models with mass below  $3.5 - 4M_{\odot}$  produce oxygen-rich ejecta (see Fig. 3), because TDU prevails over HBB. In analogy with carbon, we find that in the  $Z = 3 \times 10^{-4}$  models the increase in the surface oxygen is larger. This can be clearly seen in the difference between the increase

in [O/Fe] found in the low-mass ( $M \leq 3M_{\odot}$ ) models of  $Z = 3 \times 10^{-4}$  (left panel of Fig. 3), and the corresponding models of  $Z = 8 \times 10^{-3}$  (right panel).

The oxygen yield becomes negative (i.e. [O/Fe] below +0.4 for  $Z = 3 \times 10^{-4}$ , and +0.2 for  $Z = 8 \times 10^{-3}$ ) for  $M \geq 4M_{\odot}$ , where HBB destroys part of the surface oxygen. The effects of HBB can be seen in the decreasing trend of the surface oxygen found for  $M \geq 4M_{\odot}$  for both metallicities.

Because there is no way to produce oxygen efficiently via p-capture nucleosynthesis, the history of oxygen under the effects of HBB is a pure destruction process, that proceeds at a higher rate for larger HBB temperatures. This motivates the smaller oxygen in the ejecta of lower  $Z$  models, and also the decreasing trend with mass for  $M \geq 4M_{\odot}$  (see right panel of Fig. 2). The comparison among lines corresponding to massive AGBs in the two panels of Fig. 3 shows that oxygen is destroyed much more strongly in the  $Z = 3 \times 10^{-4}$  case (note the different scales of the two panels).

The lowest oxygen abundances in the ejecta are found for  $M \sim 6M_{\odot}$ , with [O/Fe] =  $-0.8$  (note that considering the initial [O/Fe] = +0.4 for this mixture, this corresponds to a reduction factor  $\sim 20$ ). The trend with mass becomes increasing in the SAGB regime, despite these models experience a stronger HBB (see right panel of Fig. 2). This behaviour, discussed in Ventura & D’Antona (2011), is due to the large mass loss rates experienced by SAGBs, that lose their envelope before a great destruction of the surface oxygen occurs. Both panels of Fig. 3 show that the variation of [O/Fe] with mass becomes less steep for  $M \geq 6M_{\odot}$ , confirming that the mass loss rate of the largest masses is the key-factor for the larger oxygen in the ejecta of SAGBs.

That mass loss is the key-quantity in this context is confirmed by the results we obtain by assuming a smaller parameter entering the Blöcker’s recipe,  $\eta_R = 0.005$  (corresponding to 1/4 of the standard value); the corresponding oxygen abundances in the ejecta, indicated with open

squares in Fig. 2, are consequently reduced. The results of these simulations are shown as dotted lines in Fig. 3; we see that the smaller mass loss favors ejection of oxygen-poor gas, because little mass is lost in the early AGB phases, when the surface oxygen is still large.

#### 4.2 The Mg-Al nucleosynthesis

The surface abundances of magnesium and aluminium are altered by the effects of TDU and HBB. The initial total magnesium in the stars is mainly under the form of  $^{24}\text{Mg}$ . In the regions touched by He-burning during the thermal pulses large amounts of  $^{25}\text{Mg}$  and  $^{26}\text{Mg}$  are produced, via a series of  $\alpha$ -captures, that start from  $^{14}\text{N}$ , and produce magnesium via  $^{22}\text{Ne}$ .

The effects of HBB on the magnesium abundance are more complex, due to the various proton capture reactions involving the different isotopes, ending up with the synthesis of aluminium (Siess & Arnould 2006; Izzard et al. 2007). To destroy magnesium via HBB, temperatures at the bottom of the convective zone of the order of  $T \sim 10^8\text{K}$  are needed: this is required to activate efficiently the p-capture by  $^{24}\text{Mg}$  nuclei. The outcome of magnesium burning is sensitive to the HBB temperature. When the temperature is sufficiently large, great quantities of aluminium are produced, with also the synthesis of some silicon; conversely, when the temperature is only slightly exceeding  $10^8\text{K}$ , most of the magnesium is locked in the  $^{25}\text{Mg}$  isotope, with only a modest decrease in the total magnesium (Ventura et al. 2011).

Based on the above arguments, we understand that TDU and HBB produce opposite effects on the surface magnesium: while TDU increases the Mg content, HBB favors Mg-depletion, provided that the HBB temperatures exceed  $\sim 10^8\text{K}$ . Because the initial magnesium is much larger (by  $\sim$  a factor 50) than aluminium, even a weak magnesium burning is sufficient to increase the surface aluminium.

Fig. 4 shows the magnesium (left panel) and aluminium (right) content of the ejecta of the AGB models presented in this investigation. The trend of  $[\text{Mg}/\text{Fe}]$  with mass is similar to oxygen. TDU in low-mass models favours an increase in the  $^{25}\text{Mg}$  and  $^{26}\text{Mg}$  produced in the TPDS by the chain of  $\alpha$ -captures mentioned above. In high- $Z$  models the increase in the total magnesium is negligible, given the weaker efficiency of the TDU, and the higher initial magnesium in the envelope. In the low-metallicity case the increase in the surface total magnesium is sensitive to the efficiency of the TDU, as confirmed by the difference between the lines connecting open and full squares in the left panel, indicating, respectively, the results obtained with and without extra-mixing from the borders of the PDCS.

The increase in magnesium favors a contemporary increase in the surface aluminium, because part of  $^{25}\text{Mg}$  and  $^{26}\text{Mg}$  dredged-up to the surface is converted into aluminium during the following interpulse phase.

Models dominated by HBB show a different behavior: magnesium is destroyed by a series of proton captures starting from the reaction  $^{24}\text{Mg}(p,\gamma)^{25}\text{Al}$ , that eventually lead to the formation of aluminium (see e.g. Ventura et al. (2011) for the details of the Mg-Al nucleosynthesis). The decrease in the total magnesium reaches a maximum around  $\sim 6M_{\odot}$  for the  $Z = 3 \times 10^{-4}$  models, where the destruction factor is  $\sim 0.6$  dex; in the SAGB regime the magnesium yields

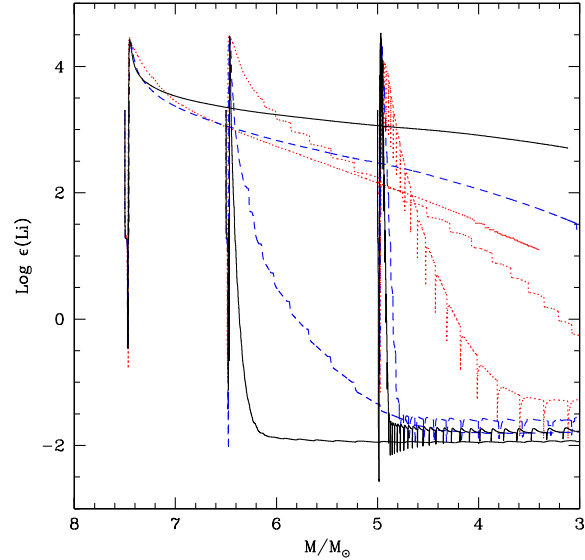


**Figure 5.** The variation during the AGB evolution of the surface lithium in models of initial mass  $5M_{\odot}$ ,  $6.5M_{\odot}$ , and  $7.5M_{\odot}$ , with metallicity  $Z = 3 \times 10^{-4}$  (black, solid line),  $Z = 10^{-3}$  (blue, dashed),  $Z = 8 \times 10^{-3}$  (red, dotted).

are higher, because mass loss is so fast to prevent great destruction of magnesium before the envelope is lost. Models achieving the greatest destruction of magnesium also produce great quantities of aluminium, whose abundance is increased by a factor  $\sim 20$  in comparison with the initial stellar content.

#### 4.3 Lithium

AGB stars are known to evolve through a phase when they are efficient lithium manufacturers. The mechanism by which lithium is produced in the envelope of these stars was first suggested by Cameron & Fowler (1971), and is activated whenever the temperature at the bottom of the convective envelope reaches  $\sim 40\text{MK}$ . Under these conditions  $\alpha$ -capture by  $^3\text{He}$  nuclei begins, with the production of beryllium, which decays into lithium; because the time-scale for beryllium decay is  $\sim 60\text{d}$ , part of the lithium is produced in the outermost and cooler regions of the envelope, where it survives to proton fusion.

Sackmann & Boothroyd (1992) first found that lithium could be produced within the context of AGB modeling, provided that a diffusive approach is used to couple nuclear burning and mixing of chemicals in regions unstable to convection. Mazzitelli et al. (1999) confirmed that lithium production can be activated efficiently when convection is modelled according to the FST treatment, in all models with mass  $M \geq 3M_{\odot}$ .

While the lithium-rich phase is crossed by all high-mass AGB models, the amount of lithium which they eject into the interstellar medium is highly uncertain. The recent analysis by D’Antona & Ventura (2009) outlines the various factors affecting the lithium content of the AGBs ejecta. The uncertainty of the results obtained stems from the fact that lithium production stops when the surface  $^3\text{He}$  is consumed:



the quantity of lithium expelled is determined by the mass lost by the star during the phase when it is lithium-rich.

The recent investigation by Ventura & D’Antona (2010) stressed that the lithium yields by SAGBs are even more uncertain. When the same slope of the mass loss vs luminosity relation used for AGBs is adopted, SAGB models are found to produce an extremely lithium-rich gas, because most of the mass is lost before  ${}^3\text{He}$  is consumed completely. However, this latter finding is extremely sensitive to the mass loss rate adopted in the early thermal pulses experienced, after the formation of the ONe core.

The models presented in Ventura & D’Antona (2010) are compared with those in the present investigation in Fig. 5. For clarity sake, we only show three models of initial mass  $5M_{\odot}$ ,  $6.5M_{\odot}$ , and  $7.5M_{\odot}$ .

Lithium production is achieved by all the masses shown in Fig. 5, for the three metallicities investigated. For the models of  $5M_{\odot}$  and  $6.5M_{\odot}$  the lithium content expected in the ejecta is directly correlated to metallicity: higher  $Z$  models, for a given mass, experience a softer HBB, thus  ${}^3\text{He}$  is consumed more slowly, and the duration of the lithium-rich phase is longer.

In the range of mass  $4M_{\odot} \leq M \leq 6M_{\odot}$  (see Table 1) the average lithium in the ejecta is  $\log(\epsilon(Li)) \sim 2$  for  $Z = 3 \times 10^{-4}$  and  $Z = 10^{-3}$ , increasing to  $\log(\epsilon(Li)) \sim 2.5$  for  $Z = 8 \times 10^{-3}$ .

Moving from the AGB to the SAGB regime we see that the lithium yields increase with mass, as also evident from Fig. 5: this is consistent with the arguments given above.

#### 4.4 Which implications for the self-enrichment of Globular Clusters?

Massive AGBs and SAGBs have been proposed as one of the possible polluters of the interstellar medium in Globular Clusters: from the gas ejected by these sources new stars would form, with the chemistry of their ejecta. This is the reason why it is extremely important to understand which are the predicted yields of these stars in terms of the elements commonly investigated in the spectroscopic surveys of GC stars, i.e. oxygen, sodium, magnesium, aluminium and silicon.

The O–Na anticorrelation is a common feature of all the galactic GCs so far examined, though the extension of the observed pattern differs from cluster to cluster. The Mg–Al trend is also a rather common feature, although a smaller amount of data are available, and in a few clusters the trend itself is not completely clear (Carretta et al. 2009).

The yields of the models presented in this investigation are shown in Fig. 6, in the O–Na (left) and Mg–Al plane (right). We also show, for completeness, the results corresponding to  $Z = 10^{-3}$  from Ventura & D’Antona (2009) and Ventura & D’Antona (2011). The O–Na trend traced by the models confirm, on qualitative grounds, the main results outlined in Ventura & D’Antona (2011) (see their Fig. 6):

- The most extreme yields, i.e. those showing the greatest depletion of oxygen, are found for the masses at the edge between the AGB and the SAGB regimes, i.e. for  $M \sim 6M_{\odot}$ . The maximum extent of the oxygen destruction is extremely sensitive to metallicity, ranging from  $\delta[O/Fe] \sim -0.3$  for

$Z = 8 \times 10^{-3}$ , to  $\delta[O/Fe] \sim -0.8$  for  $Z = 10^{-3}$ , up to  $\delta[O/Fe] \sim -1.3$  for  $Z = 3 \times 10^{-4}$ .

- Oxygen and sodium are correlated in all cases. In models where a strong destruction of oxygen occurs, the bottom of the surface convective zone is exposed to advanced p-capture nucleosynthesis at temperatures  $T > 100\text{MK}$ : in this range of T’s the destruction channel for sodium is dominant compared to the production reaction by p-capture on  ${}^{22}\text{Ne}$  nuclei, thus the sodium previously accumulated at the surface is destroyed. The oxygen yields are negative, because HBB destroys oxygen; conversely, sodium can be produced, because of the initial increase in the surface sodium determined by the second dredge-up and by the  ${}^{22}\text{Ne}$  burning via proton capture. Note that the positive correlation between oxygen and sodium is expected independently of all the uncertainties affecting the predictions concerning the sodium yield (initial neon and sodium abundances, cross-sections of the Ne–Na nucleosynthesis), that may eventually shift upwards or downwards the trend defined in Fig. 6, without changing the slope.

These results confirm that if massive AGBs were the polluters of the intra cluster medium in GCs, providing the gas from which new stellar generations formed, a certain amount of dilution of the gas ejected via stellar winds with pristine, uncontaminated matter is required, otherwise no O–Na anticorrelation can be produced.

Also, the GCs harboring a stellar generation formed directly from the ejecta of massive AGBs, with no dilution with pristine gas, must show a correlation of the lowest oxygen abundances with metallicity, more metal-poor GCs showing the most oxygen-poor population. In these stars we do not expect any sodium enhancement.

Turning to the Mg–Al cycling, we first note from the right panel of Fig. 6 that only a modest reduction of the surface magnesium is achieved in all cases, whereas some aluminium production, limited to +0.3 dex, occurs. This confirms that magnesium destruction requires temperatures exceeding  $\sim 10^8\text{K}$ , only marginally reached by the  $Z = 8 \times 10^{-3}$  models (see right panel of Fig. 1).

Both the  $Z = 10^{-3}$  and the  $Z = 3 \times 10^{-4}$  models produce magnesium-poor matter, the maximum reduction factor being, respectively,  $\delta[\text{Mg}/\text{Fe}] = -0.3$  and  $\delta[\text{Mg}/\text{Fe}] = -0.6$ . Similarly to oxygen, we find that the most extreme chemistry is not found for the most massive, SAGB models, because in the context of the present modeling these latter lose their envelope very rapidly, before a very advanced Mg–Al nucleosynthesis may occur.

The magnesium depletion is accompanied by an increase in the surface aluminium. The Al content in the ejecta reaches a threshold value of  $[\text{Al}/\text{Fe}] \sim 1.2$ , independently of the metallicity, and of the extent of the magnesium depletion. This is the effect of the balance reached between the production and destruction channels, that eventually leads to the formation of some silicon.

The uncertainties affecting the extent of magnesium depletion and aluminium enhancement were discussed in details by Ventura et al. (2011). The main outcome of this investigation is that massive AGBs in the low- $Z$  domain reach at the bottom of the surface convection zone temperatures sufficiently large to destroy  ${}^{24}\text{Mg}$ , thus their ejecta are predicted to show large  ${}^{25}\text{Mg}/{}^{24}\text{Mg}$  and  ${}^{26}\text{Mg}/{}^{24}\text{Mg}$  iso-

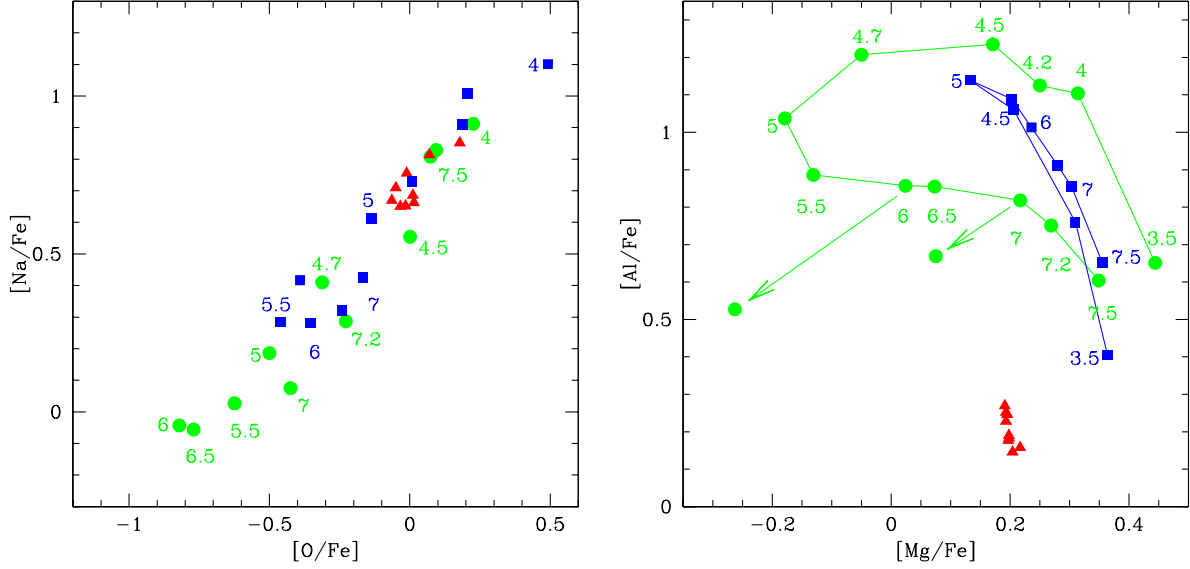


**Figure 6.** Yields of models of different metallicities in the O–Na and Mg–Al planes. Green points:  $Z = 3 \times 10^{-4}$ ; blue squares:  $Z = 10^{-3}$  models by Ventura & D’Antona (2009, 2011); red triangles:  $Z = 8 \times 10^{-3}$ . Numbers close to the points indicate the values of the initial mass. The two arrows in the right panel indicate the results from  $Z = 3 \times 10^{-4}$  models of initial mass  $6M_{\odot}$  and  $7M_{\odot}$  calculated with a smaller rate of mass loss.

topic ratios. The maximum depletion of the total magnesium was found to be determined by the cross section of the  $^{25}\text{Mg}(p,\gamma)^{26}\text{Al}$  reaction in the range of temperatures around  $\sim 10^8\text{K}$ , an increase by a factor 2 in the reaction rate corresponding to a further  $\sim -0.2$  dex in the magnesium depletion (see Fig. 5 in Ventura et al. (2011)). Even a larger Mg–depletion would scarcely influence the Al–enhancement, due to the afore mentioned equilibrium established between production and destruction rates, once Al increases by a factor  $\sim 10$ .

## 5 COMPARISON WITH OTHER INVESTIGATIONS IN THE LITERATURE

The recent years have seen a growing interest towards AGB modeling. Several research groups have contributed to produce an impressive series of models, spanning a wide range of mass and metallicities. Some of these investigations were focused on the efficiency of mixing in low–mass AGBs, and on the treatment of the borders at the convective/radiative interface (Cristallo et al. 2009; Stancliffe & Jeffery 2007). These studies complete the previous investigations on these evolutionary phases by Karakas & Lattanzio (2003, 2007), Weiss & Ferguson (2009), and the most recent update by Karakas (2010).

On the side of SAGB modeling, the recent works by Siess (2006, 2007, 2010) provided a complete and exhaustive update of the pioneering explorations focused on the physics of carbon ignition in regime of partial degeneracy, by Ritossa et al. (1996, 1999), Garcia Berro et al. (1997), Iben et al. (1997).

Among the above investigations on the AGB phase, we decided to compare our results with those by Karakas (2010) (K10): in this compilation, the yields of models with mass in the range  $M_{\odot} \leq M \leq 6M_{\odot}$ , and metallicities in the range

$0.0001 \leq Z \leq 0.02$  are presented and discussed. K10 yields are indicated in Fig. 2 and 4 with blue triangles: the open points indicate the  $Z = 8 \times 10^{-3}$  metallicity (to be compared with the red points in our compilation), whereas full points refer to  $Z = 10^{-4}$  (among the various metallicities treated in K10, this is the closest to the  $Z = 3 \times 10^{-4}$  case discussed here).

As for the SAGB phase, the most complete investigation currently present in the literature is by Siess (2010) (hereinafter S10), which treats the same chemistry as K10, with masses in the range  $7.5M_{\odot} \leq M \leq 10M_{\odot}$ , i.e. those undergoing carbon ignition in conditions of partial degeneracy. The corresponding points are indicated as open pentagons ( $Z = 8 \times 10^{-3}$ ) and asterisks ( $Z = 10^{-4}$ ) in Figs. 2 and 4.

For what concerns carbon, for masses  $M \leq 3M_{\odot}$ , and metallicity  $Z = 8 \times 10^{-3}$ , our yields for models calculated with some extra–mixing from the PDCS are rather similar to those by Karakas (2010). The reason for this is in the similarity of the physical properties of the two sets of models in this range of mass. A comparison with the models presented in Karakas et al. (2002) shows that for any given initial mass the core masses at the first TP are very close, whereas the minimum core mass at which TDU occurs is  $\sim 0.02M_{\odot}$  larger in our case. The investigations by Izzard et al. (2004) and Marigo & Girardi (2007) showed that to reproduce the luminosity function of carbon stars in the Large Magellanic Cloud, whose metallicity is similar to  $Z = 8 \times 10^{-3}$ , the core masses when the first TDU occurs must be  $\sim 0.07 - 0.1M_{\odot}$  smaller than in Karakas et al. (2002). This means that the carbon yields found in the low–mass models presented here must be considered as lower limits.

In the low–metallicity case the K10 carbon yields are a factor  $\sim 3$  higher than ours; certainly the smaller metallicity upon which the computations by K10 are based ( $Z = 10^{-4}$  vs  $Z = 3 \times 10^{-4}$ ) plays a role here, although other factors,

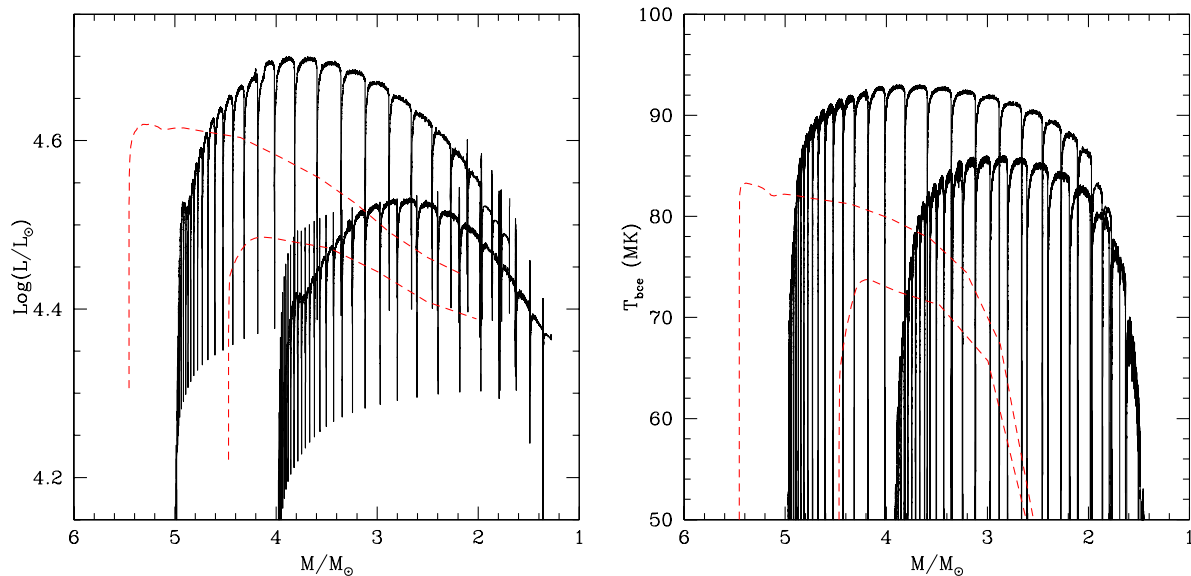


**Figure 7.** The evolution during the AGB phase of luminosity (left) and temperature at the bottom of the envelope (right) of models from the present investigation of initial mass  $4M_{\odot}$  and  $5M_{\odot}$  (black, solid tracks), and models by K10 with initial mass  $4.5M_{\odot}$  and  $5.5M_{\odot}$  (red, dashed lines). The initial masses were chosen such that the models have the same core mass at the first thermal pulse.

such as a different efficiency of TDU, cannot be ruled out as possible reasons for this difference. In both compilations we see a decrease with mass in the carbon content of the ejecta, although in the models presented here the carbon yields become negative (i.e. the average carbon content of the ejecta is smaller as it was initially), whereas in K10 models  $[\text{C}/\text{Fe}]$  hardly reaches 0, rather it remains above 2 in the low- $Z$  case. This finding outlines the main difference between the models presented here and those by K10, i.e. the extent of HBB, much stronger in our case, because of the large convective efficiency predicted by the FST treatment; K10 models are based on the MLT treatment with  $\alpha = 1.75$ , which leads to a much weaker HBB (Ventura & D’Antona 2005).

Fig. 7 compares the evolution of our models with metallicity  $Z = 8 \times 10^{-3}$  (black, solid lines) with those of the same metallicity by K10 (red, dashed tracks). The initial masses are slightly different, to compare models with the same core mass at the beginning of the AGB phase: our  $4M_{\odot}$  and  $5M_{\odot}$  cases correspond, respectively, to masses  $4.5M_{\odot}$  and  $5.5M_{\odot}$  in K10. The differences in the HBB experienced can be clearly seen in the comparison of the temperatures at the base of the envelope (see right panel): models by K10 are  $\sim 20\text{MK}$  cooler than ours. This is also related to the different luminosity of the models (see right panel of Fig. 7). Our models, evolving at larger luminosities, also suffer a larger mass loss, thus experience a smaller number of thermal pulses: we find a total of 35 and 37 TPs for  $M = 4M_{\odot}$  and  $M = 5M_{\odot}$ , to be compared to 38 TPs experienced by the K10  $4.5M_{\odot}$  model, and 56 TPs in the  $5.5M_{\odot}$  case.

HBB also affects the oxygen yields, as can be seen in the right panel of Fig. 2. In the  $Z = 8 \times 10^{-3}$  case we see that our models show some depletion of oxygen, by  $\sim 0.2 - 0.3\text{dex}$ , not found in the investigation by Karakas (2010). The most striking difference is however found in the low- $Z$  case: while in the models presented here the ejecta are predicted to

be extremely poor in oxygen, with a maximum depletion factor of the order of  $\sim 30$ , in the K10 study we obtain, independently of the mass, oxygen-enriched matter, with  $[\text{O}/\text{Fe}] > +0.4$ . To understand this difference we compared in details the most massive model in the K10  $Z = 10^{-4}$  set, i.e.  $M = 6M_{\odot}$ , with our  $Z = 3 \times 10^{-4}$  model of the same core mass, i.e.  $M = 5.5M_{\odot}$ . As in the previous comparison at larger metallicities, we find the same difference of  $\sim 20\text{MK}$  (100MK in K10, and 120MK in our case) between the maximum temperatures experienced at the bottom of the convective envelope. These different temperatures would explain the larger depletion of oxygen in our exploration, but not the large oxygen content in the K10 yields; this latter is due to the relevant contribution from TDU, partly due to the smaller metallicity of K10 models, and also to the much larger number of TPs experienced (the total number of TPs in K10 and our model are, respectively, 109 and 54).

The differences outlined above have also a feedback on the amount of nitrogen that these stars produce. Upon discussing the CNO yields, we stressed that the most efficient production of nitrogen takes place when TDU and HBB are both operating during the AGB evolution, because carbon transported outwards by TDU is later converted into nitrogen. While in our case this overproduction of nitrogen is restricted to masses  $M \sim 2.5 - 3M_{\odot}$  (more massive stars experience only a small number of thermal pulses, due to the strong HBB), in K10 this behavior is shared by practically all masses, as can be understood from the position of the full triangles in the middle panel of Fig. 2.

In the comparison with the work by Siess (2010), we preliminary note that the difference in the masses involved are due to the difference in the treatment of the convective borders during the main sequence phase of hydrogen burning. We assumed some overshoot from the border of the convective core, whereas S10 models were calculated with no extra-

mixing; similar results are obtained for a mass  $\sim 1.5 - 2M_{\odot}$  larger in Siess' computations, as can be seen in Fig. 2.

Other than the shift in the initial mass, the  $Z = 8 \times 10^{-3}$  models from the two compilations are fairly similar. In particular, we note that the maximum temperature reached at the bottom of the envelope ranges between  $\sim 10^8$  K to  $\sim 1.2 \times 10^8$  K (compare the values in the 7th col. of Tab. 1 with those of col.15 in Siess (2010)). This is the reason for the similarity in the CNO yields at this metallicity. At these temperatures HBB is sufficiently strong to destroy carbon, and to synthesize nitrogen; oxygen is only marginally touched.

Turning to the low-metallicity regime, the  $Z = 3 \times 10^{-4}$  yields presented here are rather different from those of  $Z = 10^{-4}$  by Siess (2010). While in our case we find  $-0.5 < [\text{O}/\text{Fe}] < 0$ , in the S10 work it is  $-2 < [\text{O}/\text{Fe}] < -1$ . The reason for this difference is twofold. On one hand, we see by comparing the temperatures reached at the bottom of the envelope of our models with their counterparts in the S10 compilation that these latter experience a much stronger HBB, owing to the smaller metallicity. Also, in analogy with what found in Ventura & D'Antona (2011), we stress the importance of the different treatment of mass loss: the Blöcker prescription used here leads to higher rates compared to the Vassiliadis & Wood (1993) treatment used by Siess (2010); our models lose their envelope before a great reduction of the surface oxygen is achieved. This is also clear in the difference in the number of TPs, which exceeds 2000 in S10, while it barely reaches 50 in our SAGB models. A confirmation of this comes from the results from computations of models of  $6M_{\odot}$  and  $7M_{\odot}$  where the free parameter entering the Blöcker formula was reduced to  $\eta_R = 0.005$ , simulating a reduction of 75% of the mass loss rate: the corresponding oxygen yields, indicated with open squares in the right panel of Fig. 2, confirm that more oxygen-poor ejecta are produced when the mass loss rate is decreased.

Among the various elements involved in p-capture nucleosynthesis, the evolution of the surface magnesium, and the amount of this element in the ejecta, is the most sensitive to the details of the modeling of the AGB phase. This can be seen in the right panel of Fig. 4, where our yields are compared with those by Karakas (2010) and Siess (2010). In analogy with the CNO elements, the yields corresponding to the  $Z = 8 \times 10^{-3}$  chemistry are similar, whereas those for the low metallicity models are extremely different. For  $M \leq 3.5M_{\odot}$  an increase in the magnesium content of the ejecta is found both in our models and in those by Karakas (2010); these latter predict a larger enrichment in magnesium, partly due to the smaller metallicity adopted. The magnesium yields of more massive stars are completely different: while our models, experiencing strong HBB, show a reduction of the initial magnesium, up to  $-0.6$  dex at  $\sim 5M_{\odot}$ , the K10 yields are magnesium-rich, confirming the difference in the efficiency of the HBB experienced, and in the relative role played by HBB and TDU. Both our and K10 models are found to be Al-rich, as a consequence of the conversion of magnesium to aluminium via p-capture during the interpulse phase.

In the SAGB domain, the differences with respect to the models by Siess (2010) reflect the situation already found in the analysis of the oxygen content of the ejecta. Because of the smaller mass loss experienced, the yields by Siess (2010)

are more Mg-poor, because there is more time available to destroy the surface magnesium via HBB.

## 6 CONCLUSIONS

We present and discuss new models of stars of intermediate mass, evolved during the AGB phase, characterized by the occurrence of a series of Thermal Pulses. We also focus on the SAGB evolution, experienced by models with mass  $6M_{\odot} < M < 8M_{\odot}$ , that develop a core of oxygen and neon. These results complete previous explorations from our group, based on a single metallicity,  $Z = 10^{-3}$ , and extend to metallicities typical of low-Z Globular Clusters, i.e.  $Z = 3 \times 10^{-4}$ , and to a chemistry typical of substantially higher metallicity clusters,  $Z = 8 \times 10^{-3}$ .

In agreement with previous investigations, we find that massive models with  $M \geq 3M_{\odot}$  experience HBB, whereas in lower-mass structures the only mechanism active in changing the surface chemistry is TDU. The ejecta of low-mass AGBs are enriched in the overall C+N+O content, and also in magnesium, whereas the more massive models will reverse into the interstellar medium gas contaminated essentially by p-capture nucleosynthesis, with the depletion of the surface oxygen and magnesium, and the increase in the sodium and aluminium content.

The extent of the HBB is found to be strongly sensitive to metallicity: low-Z, massive AGBs (with  $Z = 3 \times 10^{-4}$ , roughly corresponding to  $[\text{Fe}/\text{H}] = -2$ ) reach very large temperatures at the bottom of the surface convective mantle, exceeding 100MK. The corresponding yields show a small oxygen content, up to  $\sim 20$  times lower than in the initial mixture, and a magnesium depletion of a factor  $\sim 5$ . Aluminium is increased by a factor  $\sim 10 - 20$ , which is the highest abundance achievable within the present schematization; this is because at very large temperatures the production and destruction channels compensate: at these T's, silicon synthesis is expected. The oxygen and sodium in the ejecta are correlated, because for  $T > 80$  MK oxygen depletion is accompanied by the destruction of the sodium previously accumulated by the second dredge-up, and further increased in the early AGB phase, by proton-capture on  $^{22}\text{Ne}$  nuclei.

The  $Z = 8 \times 10^{-3}$  massive AGB models experience only a modest HBB, thus the ejecta are expected to produce much less contaminated ejecta: magnesium is hardly touched by the HBB nucleosynthesis, whereas the depletion of oxygen barely exceeds a factor  $\sim 2$ .

In the low-mass regime, where the surface chemistry is unaffected by HBB, the results presented here are in good agreement with other investigations in the literature, although the extent of the carbon enrichment is sensitive to the details of the treatment of the convective borders. For more massive models, the results depend on the combined effects of the description of convection and on the mass loss treatment. While the enhancement of nitrogen and aluminium appear as rather robust, the extent of magnesium and oxygen depletion are strongly model dependent, as the sodium content, which is also affected by the uncertainties in the relevant cross-sections.

Two main results found in the investigations by Ventura & D'Antona (2011) are confirmed here, independently of metallicity:

- The helium content of the ejecta increases with mass, reaching  $Y \sim 0.38$  in the more massive models, in the SAGB regime.

- The models showing the most extreme chemistry are those with mass  $M \sim 6M_{\odot}$ , at the edge between the AGB and SAGB regimes. This is due to the large mass loss experienced by SAGBs, that lose their envelopes before a very advanced HBB nucleosynthesis is experienced.

## ACKNOWLEDGMENTS

The authors are indebted to the referee, Achim Weiss, for the careful reading of the manuscript, and for the competent comments and suggestions, that contributed to increase the quality of this work. This work was partially funded by the PRIN INAF 2009 "Formation and Early Evolution of Massive Star Clusters".

## REFERENCES

- Angulo C., Arnould M., Rayet M., et al., 1999, Nucl.Phys. A, 656, 3
- Blöcker T., 1995, A&A, 297, 727
- Blöcker T., 1991, A&A, 244, L43
- Boothroyd A. I., Sachmann, I. J. 1988, ApJ, 328, 653
- Bowen G.H., 1988, ApJ, 329, 299
- Cameron A.G.W., Fowler W.A., 1971, ApJ, 164, 111
- Canuto V.M.C., Mazzitelli I., 1991, ApJ, 370, 295
- Carretta E., Bragaglia A., Gratton R., et al., 2009, A&A, 505, 117
- Cloutmann, L., & Eoll, J.G. 1976, ApJ, 206, 548
- Cristallo S., Straniero O., Gallino R., Piersanti L., Dominguez I., Lederer M. T. 2009, ApJ, 696, 797
- D'Antona, F., Bellazzini, M., Caloi, V., Pecci, F. F., Galieti, S., & Rood, R. T. 2005, ApJ, 631, 868
- D'Antona, F., Ventura P. 2009, in Proceedings of the IAU Symposium No. 268, "Light element in the Universe", Charbonnel, Tosi, Primas & Chiappini editors.
- D'Ercole A., Vesperini E., D'Antona F., Mc Millan S.L.W., Recchi S. 2008, MNRAS, 391, 825
- D'Ercole A., D'Antona F., Ventura P., Vesperini E., Mc Millan S.L.W. 2010, MNRAS, 407, 854
- D'Ercole A., D'Antona, F., Vesperini E. 2011, MNRAS, 415, 1304
- D'Ercole A., D'Antona F., Carini R., Vesperini E., Ventura P., 2012, MNRAS, 423, 1521
- Di Criscienzo M., Ventura P., D'Antona F. 2010a, A&A, 511, 70
- Di Criscienzo M., Ventura P., D'Antona F., Milone A., Piotto G. 2010b, MNRAS, 408, 999
- Fenner Y., Campbell, S., Karakas, A.I., Lattanzio, J.C., Gibson, B.K., 2004, MNRAS, 353, 789
- Ferraro A.D., Gail H.P., 2006, A&A, 553, 576
- Formicola A., Imbriani G., Costantini H., et al. 2004, Phys. Lett. B, 591, 61
- Fynbo H. O. U. et al. 2005, Nature, 433, 136
- Gail H.P., Sedlmayr E., 1999, A&A, 347, 594
- Garcia Berro E., Ritossa C., Iben I. J. 1997, ApJ, 485, 765
- Gratton R., et al. 2001, 1998, A&A, 369, 87
- Grevesse N., Sauval A.J, 1998, SSRv, 85, 161
- Hale S. E., Champagne A. E., Iliadis C., et al. 2002, Phys. Rev. C, 65, 5801
- Hale, S. E., Champagne, A. E., Iliadis C., et al. 2004, Phys. Rev. C, 70, 5802
- Herwig F. 2000, A&A, 360, 952
- Iben I. J. 1975, ApJ, 196, 525
- Iben I. J., Ritossa C., Garcia Berro E. 1997, ApJ, 489, 772
- Iglesias C. A., Rogers F. J., 1996, ApJ, 464, 943
- Izzard R., Tout C.A., Karakas A.I., Pols O.R., 2004, MNRAS, 350, 407
- Izzard R., Lugaro M., Karakas A.I., Iliadis C., van Raai M., 2007, A&A, 466, 641
- Karakas A.I. 2010, MNRAS, 403, 1413
- Karakas A.I., Lattanzio J.C., Pols O.R., 2002, PASA, 19, 515
- Karakas A.I., Lattanzio J.C., 2003, PASA, 20, 279
- Karakas A.I., Lattanzio J.C., 2007, PASA, 24, 103
- Kunz R., Fey M., Jaeger M., Mayer A., Hammer J. W., Staudt G., Harissopulos S., Paradellis T. 2002, ApJ, 567, 643
- Marigo P., Girardi L., 2007, A&A, 469, 239
- Marigo P., Aringer B., 2009, A&A, 508, 1539
- Mazzitelli I., D'Antona F., Ventura P. 1999, A&A, 348, 846
- Piotto G., Bedin L.R., Androsen J., et al., 2007, ApJ, 661, L53
- Poelarends A.J.T., Herwig F., Langer N., Heger A. 2008, ApJ, 675, 614
- Renzini A., Voli M., 1981, A&A, 94, 175
- Ritossa C., Garcia Berro E., Iben I. J. 1996, ApJ, 460, 489
- Ritossa C., Garcia Berro E., Iben I. J. 1999, ApJ, 515, 381
- Sackmann I.J., Boothroyd A.I. 1992, ApJ, 392, L71
- Saumon D., Chabrier G., Van Horn, H. M. 1995, ApJS, 99, 713
- Schwarzschild M., Harm R. 1965, ApJ, 142, 855
- Schwarzschild M., Harm R. 1967, ApJ, 145, 496
- Siess L., 2006, A&A, 448, 717
- Siess L., 2007, A&A, 476, 893
- Siess L., 2010, A&A, 512, A10
- Siess L., Arnould M. 2006, A&A, 489, 395
- Stancliffe R. J., Jeffery C. S., 2007, MNRAS, 375, 1280
- Stolzmann W., Blöcker T., 2000, A&A, 361, 1152
- van Loon J., Cioni M.R., Zijlstra A., et al. 2005, A&A, 348, 452
- Vassiliadis E., Wood P.R., 1993, ApJ, 413, 641
- Ventura P., Carini R., D'Antona F., 2011, MNRAS, 415, 3865
- Ventura P., D'Antona F., 2005, A&A, 341, 279
- Ventura P., D'Antona F., 2008, A&A, 479, 805
- Ventura P., D'Antona F., 2009, A&A, 499, 835
- Ventura P., D'Antona F., 2010, MNRAS, 402, L72
- Ventura P., D'Antona F., 2011, MNRAS, 410, 2760
- Ventura P., D'Antona F., Mazzitelli I., 2000, A&A, 363, 605
- Ventura P., D'Antona F., Mazzitelli I., Gratton, R., 2001, ApJ, 550, L65
- Ventura P., Di Criscienzo M., Schneider R., Carini R., Valiante R., D'Antona F., Gallerani S., Maiolino R., Tornambé A. 2012, MNRAS, 420, 1442
- Ventura P., Di Criscienzo M., Schneider R., Carini R., Valiante R., D'Antona F., Gallerani S., Maiolino R., Tornambé A. 2012, MNRAS, 424, 2345
- Ventura P., Marigo P., 2009, MNRAS, 399, L54

- Ventura P., Marigo P., 2010, MNRAS, 408, 2476  
Ventura P., Zeppieri A., Mazzitelli I., D'Antona F., 1998,  
A&A, 334, 953  
Wachter A., Schröder K.P., Winters J.M., Arndt T., Sedl-  
mayr E. 2002, A&A, 384, 452  
Weiss A., Ferguson J.W., 2009, A&A, 508, 1343